

## Westerbork ultra-deep survey of HI at $z=0.2$

---

**Marc Verheijen<sup>\*,a</sup>, Boris Deshev<sup>a</sup>,  
Jacqueline van Gorkom<sup>b</sup>, Bianca Poggianti<sup>c</sup>, Aeree Chung<sup>d</sup>, Ryan Cybulski<sup>e</sup>,  
K.S. Dwarakanath<sup>f</sup>, María Montero-Castaño<sup>b</sup>, Glenn Morrison<sup>g</sup>,  
David Schiminovich<sup>b</sup>, Arpad Szomoru<sup>h</sup>, Min Yun<sup>e</sup>**

<sup>a</sup> Kapteyn Astronomical Institute, University of Groningen, Groningen, The Netherlands

<sup>b</sup> Department of Astronomy, Columbia University, New York, U.S.A.

<sup>c</sup> Istituto Nazionale di Astrofisica (INAF), Osservatorio Astronomico di Padova, Padova, Italy

<sup>d</sup> Harvard-Smithsonian Center for Astrophysics, Cambridge, Massachusetts, U.S.A.

<sup>e</sup> Department of Astronomy, University of Massachusetts, Amherst, Massachusetts, U.S.A.

<sup>f</sup> Raman Research Institute, Bangalore, India

<sup>g</sup> Institute for Astronomy, University of Hawaii, Honolulu, Hawaii, U.S.A.

<sup>h</sup> Joint Institute for VLBI in Europe (JIVE), Dwingeloo, The Netherlands

E-mail: verheijen@astro.rug.nl

In this contribution, we present some preliminary observational results from the completed ultra-deep survey of 21cm emission from neutral hydrogen at redshifts  $z=0.164-0.224$  with the Westerbork Synthesis Radio Telescope. In two separate fields, a total of 160 individual galaxies has been detected in neutral hydrogen, with HI masses varying from  $1.1 \times 10^9$  to  $4.0 \times 10^{10} M_{\odot}$ . The largest galaxies are spatially resolved by the synthesized beam of  $23 \times 37 \text{ arcsec}^2$  while the velocity resolution of 19 km/s allowed the HI emission lines to be well resolved. The large scale structure in the surveyed volume is traced well in HI, apart from the highest density regions like the cores of galaxy clusters. All significant HI detections have obvious or plausible optical counterparts which are usually blue late-type galaxies that are UV-bright. One of the observed fields contains a massive Butcher-Oemler cluster but none of the associated blue galaxies has been detected in HI. The data suggest that the lower-luminosity galaxies at  $z \approx 0.2$  are more gas-rich than galaxies of similar luminosities at  $z=0$ , pending a careful analysis of the completeness near the detection limit. Optical counterparts of the HI detected galaxies are mostly located in the 'blue cloud' of the galaxy population although several galaxies on the 'red sequence' are also detected in HI. These results hold great promise for future deep 21cm surveys of neutral hydrogen with MeerKAT, APERTIF, ASKAP, and ultimately the Square Kilometre Array.

ISKAF2010 Science Meeting - ISKAF2010

June 10-14, 2010

Assen, the Netherlands

---

\*Speaker.

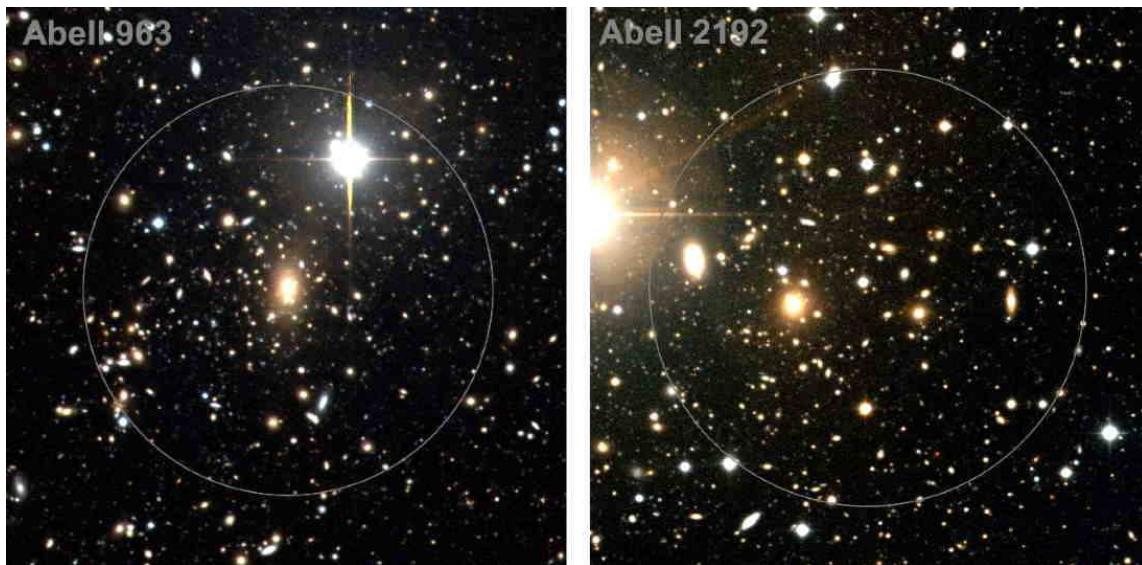


**Figure 1:** Optical images of the galaxy clusters Abell 963 at  $z=0.206$  (left) and Abell 2192 at  $z=0.188$  (right). The colours are constructed from deep B- and R-band images acquired with the Wide Field Camera of the Isaac Newton Telescope. Although the entire  $1 \text{ deg}^2$  of the primary beam of the WSRT was imaged, these images only show an area of  $6.8 \times 6.8 \text{ arcmin}^2$  centered on the clusters. The large circles have a diameter of 1 Mpc at the distances of these clusters.

## 1. Introduction

It is important to understand the role and fate of neutral hydrogen as a basic ingredient of the formation process of galaxies and as a sensitive tracer of subsequent evolutionary processes, both over cosmic time and in different environments. In the local universe, the morphology and kinematics of the cold atomic gas in and around galaxies often reveal physical mechanisms such as tidal interactions, ram-pressure stripping and ‘cold accretion’ that are very difficult to detect by other observational means (e.g. van der Hulst, this issue). Furthermore, these mechanisms are strongly influenced by the particulars of the local and global environments in which galaxies reside.

The predominance and efficiency of such processes are likely to evolve over cosmic time. For instance, the overall star formation density in the universe has declined by an order of magnitude in the last 6 Gyr while the morphological mix of galaxy populations has changed significantly, especially in the dense environments of galaxy clusters. The fraction of blue galaxies in clusters was higher in the past (e.g. Butcher & Oemler, 1978) while the relative number of spiral galaxies in clusters increases with redshift, at the expense of the S0 population (e.g. Fasano et al 2000).

At a redshift of 0.2 or a look-back time of 2.5 Gyr, signatures of cosmic evolution of the galaxy populations become evident. The nearest Butcher-Oemler (B-O) clusters are found at  $z \approx 0.2$  and one of the many questions one could ask, is whether the B-O effect relates to the rate at which galaxy clusters accrete their members or whether it is caused by the accreted population of field galaxies that may be more gas-rich as these redshifts. To address this issue and many others, like the cosmic evolution of the HI Mass Function and  $\Omega_{\text{HI}}$ , we set out to study the HI properties of galaxies at  $z \approx 0.2$  with the Westerbork Synthesis Radio telescope (WSRT). The goal

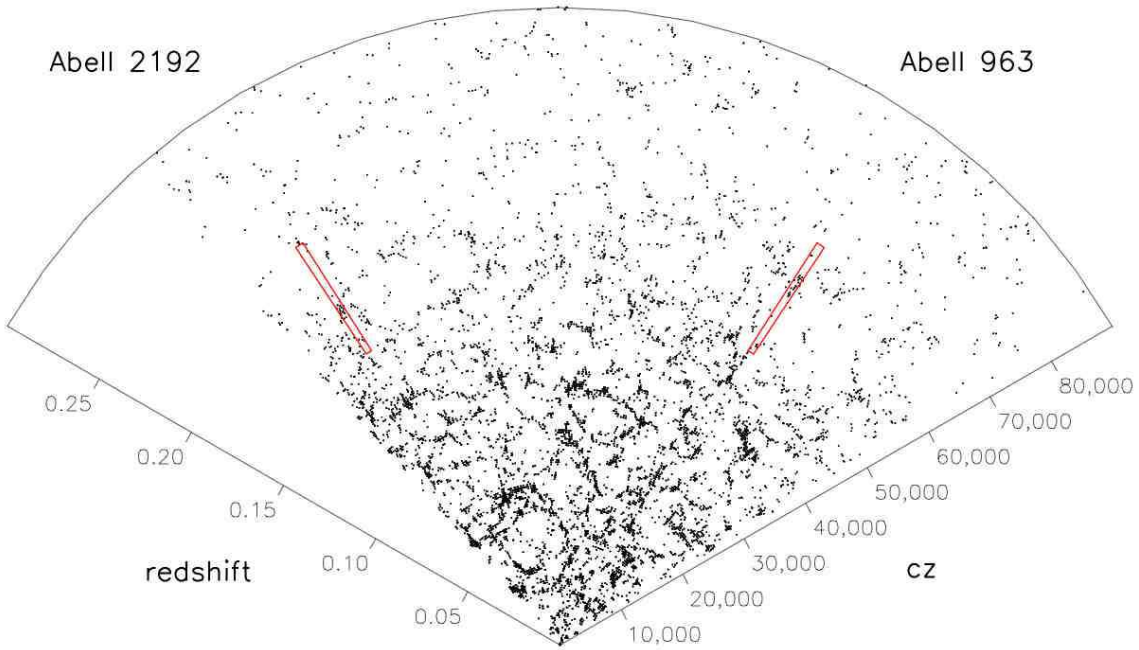


**Figure 2:** A redshift pie-diagram along a great circle passing through both clusters. Dots represent galaxies with optical redshifts from the SDSS. The elongated rectangles indicate the two volumes that have been surveyed with the WSRT, covering the redshift range 0.164–0.224. These volumes sample both overdense and underdense regions. At these redshifts, the large scale structure becomes sparsely sampled by the SDSS. Note that the HIPASS survey does not extend beyond  $cz=12,000$  km/s while the Alfalfa survey with the Arecibo telescope is restricted to  $z \lesssim 0.06$ .

is to relate the HI characteristics of the galaxies to their luminosities, morphologies, star formation rates, the evolutionary state of their constituent stellar populations, as well as to their global and local environments.

## 2. Target fields

Two single-pointing fields were selected in the northern sky, each containing an Abell cluster of galaxies and the large scale structure in which they are embedded, as well as foreground and/or background voids, thus sampling the broadest range of cosmic environments. Abell 963 at  $z=0.206$  is a massive lensing cluster with a strong B-O effect and an unusual large fraction of blue galaxies ( $f_B=0.19$ , Butcher et al 1983). With a velocity dispersion of  $1350 \text{ km s}^{-1}$  it is a bright X-ray source and the regular X-ray contours, centered on a central cD galaxy, suggest a low level of substructure in this cluster. Abell 2192 at  $z=0.188$  is less massive and more diffuse. The fraction of blue galaxies is yet unknown for this cluster. With a velocity dispersion of  $650 \text{ km s}^{-1}$ , this cluster is barely detected in X-rays. Figure 1 shows a color image of both clusters. It should be stressed that the galaxy clusters themselves only occupy  $\sim 4\%$  of the surveyed volumes.

Figure 2 indicates the locations of the two volumes in a pie-diagram of redshift space along a great circle through both clusters. Redshifts are taken from the SLOAN survey. Clearly, based on optical redshifts, the large scale structure is less well sampled at these distances. Note that the

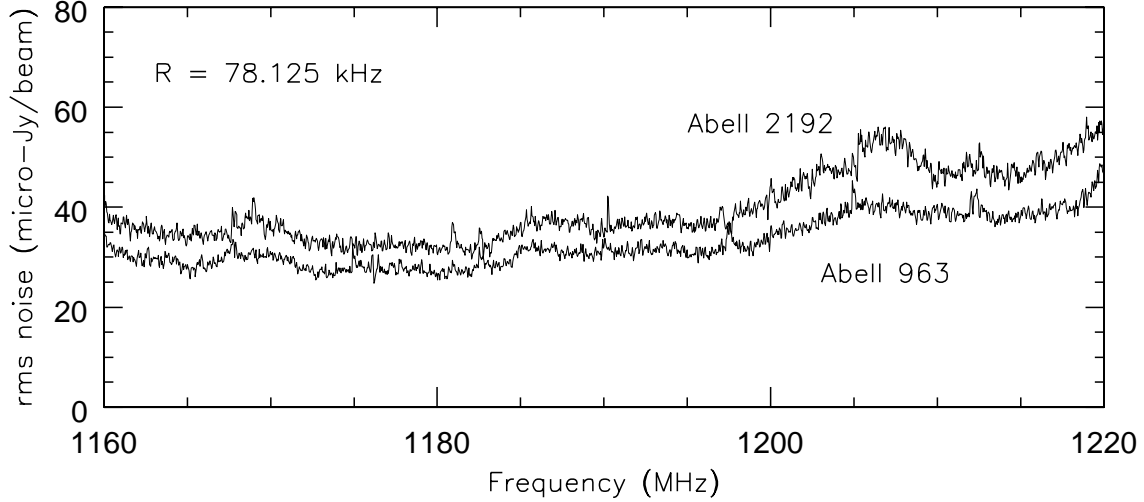


**Figure 3:** The achieved rms noise levels in the continuum subtracted data cubes as a function of frequency, after Hanning smoothing was applied to yield a FWHM spectral resolution of 78.125 kHz. Although the data for both fields was calibrated and processed independently, the rms noise in both fields shows the same trends with frequency. This is likely the result of low-level RFI that could not be removed from the individual measurements. These noise levels are close to the expected thermal noise.

blind HIPASS survey does not extend beyond  $cz=12,000 \text{ km s}^{-1}$  and that the Alfafa survey with the Arecibo telescope is limited to a maximum redshift of  $z \approx 0.06$ . The widths and depths of the volumes surveyed with the WSRT are explained in the next section.

### 3. Observations

The observations took maximum advantage of the powerful IF system and backend of the WSRT. Eight overlapping IF bands, each 10 MHz wide and with 256 dual-polarisation channels, covered the contiguous frequency range between 1220 and 1160 MHz with 1236 channels, each 39.0625 kHz wide. This corresponds to a redshift range of  $0.1643 < z < 0.2245$  or  $49,426 < cz < 67,300 \text{ km s}^{-1}$ . For  $\Omega_M=0.3$ ,  $\Omega_\Lambda=0.7$  and  $H_0=70 \text{ km s}^{-1} \text{ Mpc}^{-1}$ , this corresponds to a range in luminosity distance of  $789 < D_{\text{lum}} < 1,117 \text{ Mpc}$  or an effective volume depth of 328 Mpc. At 1190 MHz, the Full-Width-Quarter-Maximum of the primary beam of the WSRT is 61.7 arcminutes wide, or 11.9 Mpc. Consequently, the entire combined volume that has been blindly surveyed within the 60 MHz passband and the FWQM of the primary beam is  $\sim 73,000 \text{ Mpc}^3$ . This is equivalent to the volume of the Local Universe within a distance of 26 Mpc. After identifying the HI emission and cleaning of the channel maps, the synthesized beam was restored with a Gaussian beam with a FWHM of  $23 \times 37 \text{ arcsec}^2$  which corresponds to  $74 \times 119 \text{ kpc}^2$  at the center of the band.

The goal of these ultra-deep HI observations is to be able to detect, at the distance of each cluster, a minimum HI mass of  $2 \times 10^9 M_\odot$  over a  $150 \text{ km s}^{-1}$  wide emission line, with a signal-to-noise of 4 in each of three adjacent and independent spectral resolution elements. This corresponds to a limiting column density of  $3 \times 10^{19} \text{ cm}^{-2}$  over a  $80 \text{ km s}^{-1}$  wide profile at the 7-sigma level. These detection limits require a total integration time of  $78 \times 12^{\text{hr}}$  for Abell 2192 and  $117 \times 12^{\text{hr}}$  for Abell 963. The observations were collected in a 8-semester long-term Large Program during

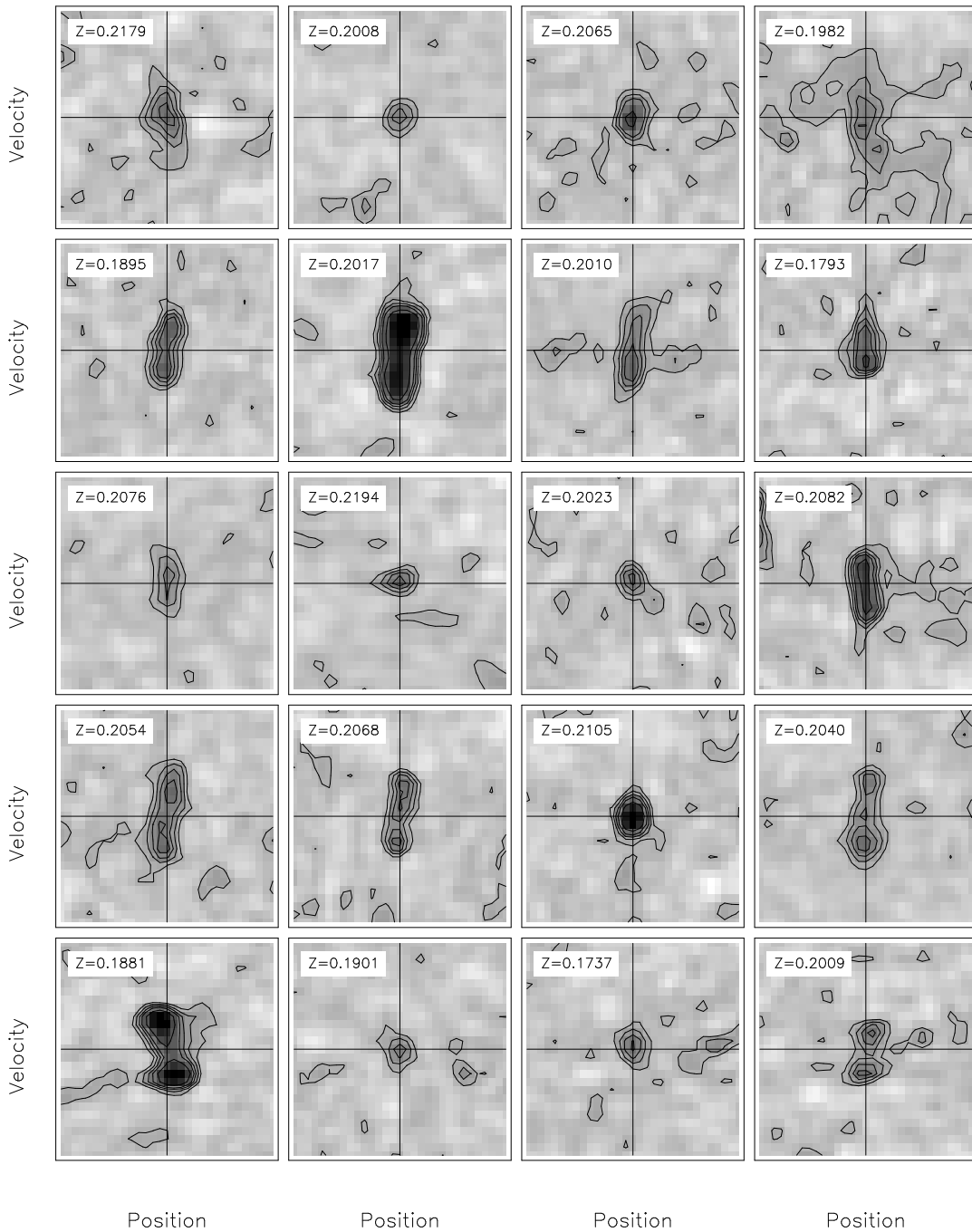


**Figure 4:** Position-velocity diagrams of 20 random HI detections. The vertical velocity axis covers  $\sim 1,000$  km/s in the rest-frame of the galaxies. The horizontal axis covers 1 arcminute on either side of the source. Horizontal lines indicate the systemic velocity, the vertical lines correspond to the central position of the HI source. Contour levels are at 1.5, 3.0, 4.5, 6.0, 9.0 and 12.0 times the local noise. The FWHM spectral resolution in these maps is 312.5 kHz, or 76 km/s at the center of the band. Not all sources fulfil the detection criteria at this particular spectral resolution. Note that many galaxies show the typical double-peaked velocity profiles and that several galaxies are spatially resolved.

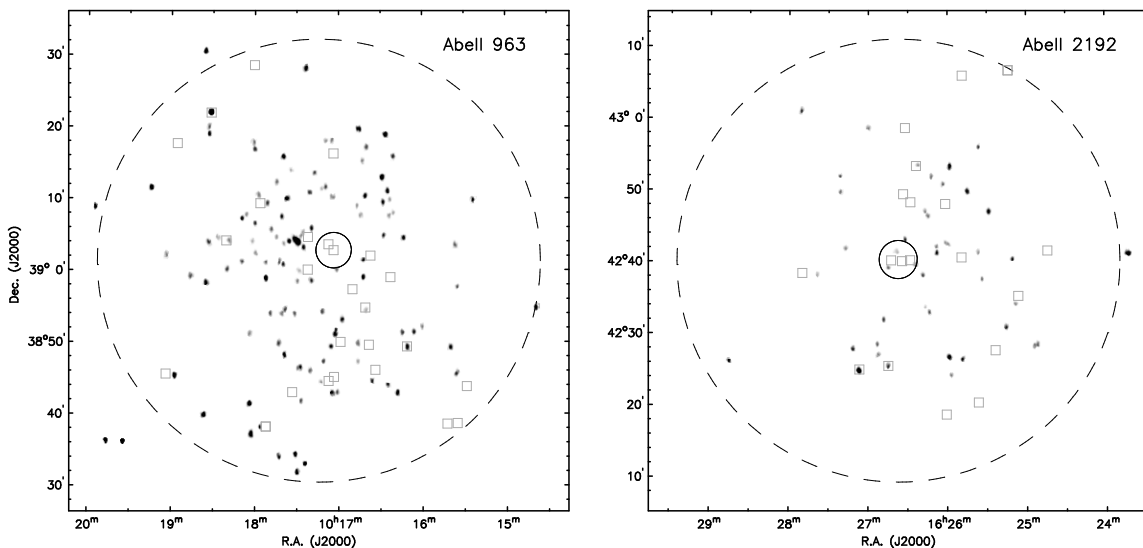


**Figure 5:** HI column density maps of the entire WSRT field-of-view, integrated over the full redshift range. HI detections are indicated by grayscales. Open squares indicate the positions of galaxies with optical redshifts from the SDSS that fall within the 0.164–0.224 redshift range. There is very little correspondence between the HI detected galaxies and the galaxies targeted for optical spectroscopy by the SDSS. The large dashed circle indicates the FWQM of the primary beam of the WSRT. The small circles near the center correspond to the circles in Figure 1.

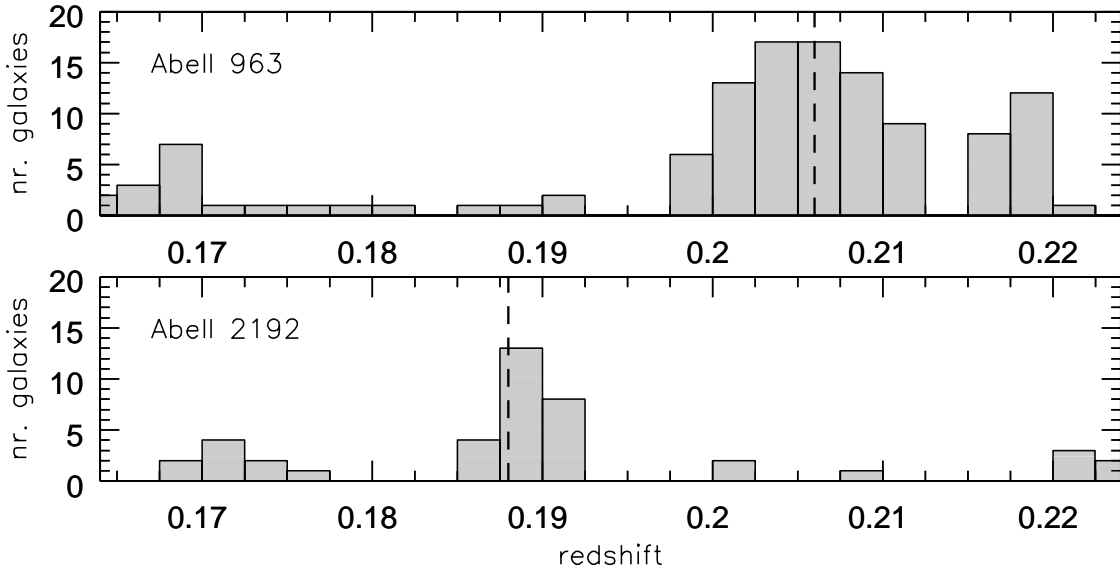
the years 2005 through 2008. First results from the pilot observations in 2005 are described by Verheijen et al. (2007).

Figure 3 shows the achieved rms noise in each continuum-subtracted data cube as a function of frequency, after Hanning smoothing to a spectral resolution of 78.125 kHz. The variations in the rms noise are a consequence of RFI residuals and frequency dependent flagging, especially above 1200 MHz. Below 1200 MHz, 5-8% of the visibilities were flagged but above 1200 MHz this was 15-17%. The measured noise levels are very close to the thermal noise that could be expected given the number of retained visibilities and the effective  $A/T_{\text{sys}}$  of the telescope. At these extremely low noise levels, imperfections in the bandpass calibration become noticeable after combining the individual measurements. In particular the position-dependent shape of the bandpass results in significant frequency-dependent residuals after subtraction of the continuum sources. Fortunately, these residuals have sufficient spatial and frequency coherence to avoid confusion with real sources, but they do affect the overall rms noise in a channel map. The non-uniformity of the noise, however, does complicate automatic source finding algorithms and corrections for incompleteness.

The deep HI observations with the WSRT are supplemented with B- and R-band imaging with the INT, NUV and FUV imaging with GALEX, 3.6, 4.5, 5.6, 8, 24 and 70 micron imaging with Spitzer, as well as optical spectroscopy with WIYN. This contribution, however, focuses on the HI observations and the optical luminosities and colours of the HI detected galaxies.

#### 4. Preliminary results

After initial Hanning smoothing, the data cubes were smoothed further to a Gaussian fre-



**Figure 6:** The redshift distributions of the HI detected galaxies in both fields. The vertical dashed lines indicate the redshifts of the clusters based on optical spectroscopy of selected cluster members. Note the overdensities in the field of Abell 963 at redshifts of 0.167, 0.205 and 0.218, and in the field of Abell 2192 at redshifts of 0.171, 0.189 and 0.221. This corresponds roughly to the large scale structure within the surveyed volumes as shown in Figure 2.

quency response with a FWHM of 4, 6 and 8 spectral channels. Thus, four data cubes exist for each field, with FWHM spectral resolutions of 78.125, 156.25, 234.375 and 312.5 kHz or 19, 38, 57 and 76 km/s at 1190 MHz.

Sources were automatically identified by searching in all data cubes for pixels above a certain threshold that are connected in frequency space. Given the structure in the noise, detection criteria were set conservatively at  $1 \times 8\sigma$ ,  $2 \times 5\sigma$ ,  $3 \times 4\sigma$ , or  $4 \times 3\sigma$ . In the latter case, four independent but connected spectral resolution elements, each at least  $3\sigma$  above the noise in a channel map, would constitute a detection. Each detection was visually inspected to avoid confusion with structure in the noise. In several cases, only one peak of a double-horned profile was detected or only part of an asymmetric HI profile was isolated by this detection algorithm. After removing spurious detections, correcting incomplete detections and verifying the presence of an optical and UV counterpart, a total of 160 galaxies was detected in HI, 118 in Abell 963 and 42 in Abell 2192. The significantly different detection rates for both fields can be ascribed to a difference in the rms noise levels, combined with cosmic variance of the large scale structure in the two volumes.

Figure 4 shows random examples of twenty position-velocity diagrams extracted from the data cubes at the lowest spectral resolution. These slices were extracted at the positions where the HI emission peaks while the angles at which these slices were taken do correspond to the position angle of the identified optical counterpart. Despite the large size of the synthesised beam, many sources are spatially resolved, indicating extended HI disks. Note that not all sources fulfil the detection criteria at this low spectral resolution. For instance, the faintest sources in the upper and bottom rows exceed the  $4 \times 3\sigma$  threshold in the data cubes with the highest spectral resolution while

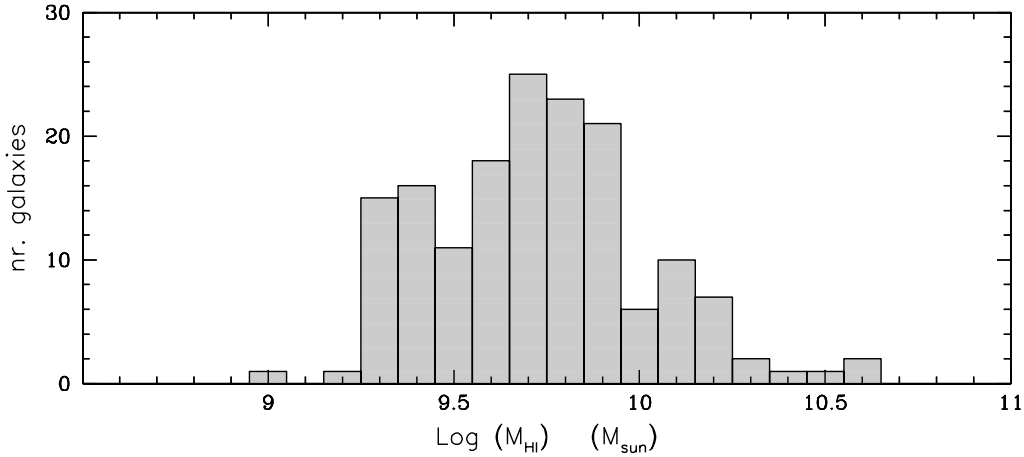


**Figure 7:** The combined distribution of detected HI masses in both volumes. The most gas-rich galaxies may be closely interacting galaxy pairs that could not be resolved by the synthesized beam of the WSRT.

they have a UV-bright optical counterpart within the FWHM of the synthesized beam.

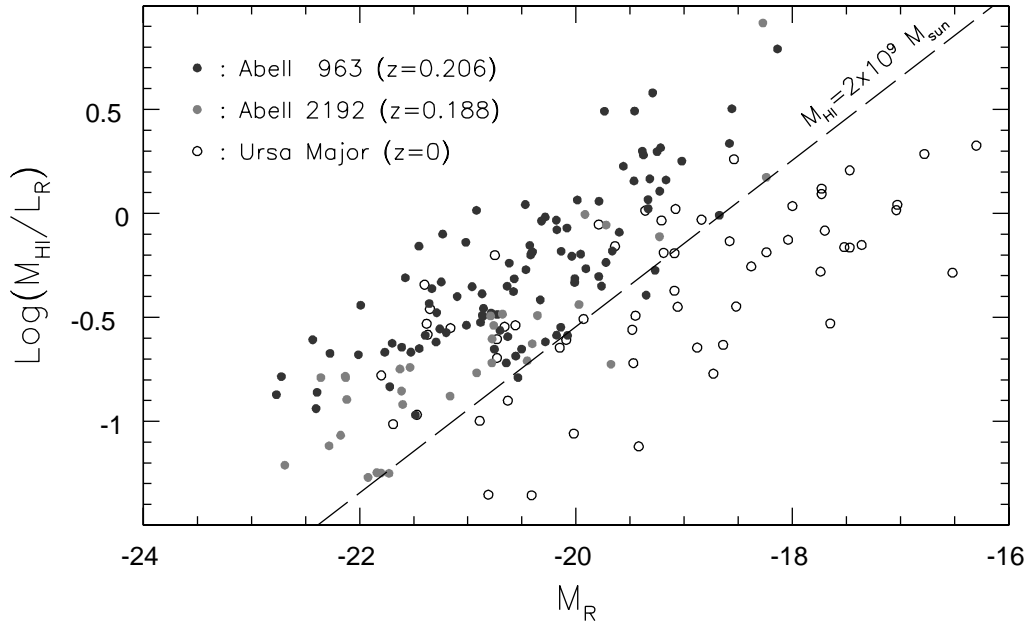
Figure 5 presents in greyscale the total HI maps of all detections in both surveyed volumes. In Abell 963, the projected density of HI detections clearly peaks towards the center of the primary beam although a few gas-rich galaxies are detected beyond the FWQM. In Abell 2192, the distribution of HI detections in the field-of-view is clearly asymmetric with most detections on the west side of the cluster. This is obviously a manifestation of the large scale structure within the surveyed volume and this seems to be corroborated by a similar asymmetric distribution of galaxies with optical redshifts from the SDSS. It should also be noted that not a single HI detection was found near the center of Abell 963. Several HI absorption systems against bright continuum sources have also been found but are not identified in this figure.

Figure 6 depicts the redshift distributions of the HI detections in both volumes. The redshifts of the clusters clearly stand out and the overall distribution is in agreement with the distribution of optical redshifts in these volumes as indicated in Figure 1. It is noteworthy that the optical redshifts of the clusters, based on optical spectroscopy of the brightest cluster members, do not coincide with the peak of the redshift distributions of the HI detections. This may indicate that the large scale structure in which these clusters are embedded may be asymmetric which is also evidenced by the total HI map for the field centered on Abell 2192.

Figure 7 shows the distribution of the 160 measured HI masses. As expected, the distribution peaks around  $M_{\text{HI}}^*$  with many detections down to the HI mass limit of  $\sim 2 \times 10^9 M_{\odot}$ . The distribution also has a remarkable tail toward the highest HI masses. Some of these detections are associated with closely interacting galaxies or compact galaxy groups that could not be resolved by the synthesized beam of the WSRT. Inspection of the optical images and the asymmetries of the global profiles will help to resolve this issue. To construct the HI Mass Function and derive  $\Omega_{\text{HI}}$  from these data requires thorough completeness corrections and an assessment of the cosmic variance to estimate the systematic uncertainties.

Figure 8 illustrates the relative gas content of the detected galaxies as a function of their abso-





**Figure 8:** The HI gas mass per solar luminosity of the HI detected galaxies versus absolute magnitude, compared with a well-studied local sample at  $z=0$  (Verheijen & Sancisi 2001). The slanted dashed line indicates the nominal detection limit at the redshifts of the clusters.

lute R-band magnitude. At zero redshift, it is well-known that the relative gas content of galaxies increases with decreasing luminosity as illustrated by the open symbols. A similar trend is observed at  $z \approx 0.2$  and at face value, this trend seems to be even steeper with the fainter galaxies being even more gas-rich. This, however, could be the result of the detection limit of the observations as indicated by the slanted dashed line. To confirm the suggestion that low-mass galaxies are more gas-rich at higher redshifts, requires a careful investigation of the completeness near the detection limit. This will be investigated in the near future.

Figure 9 presents a combined colour-magnitude diagram of all galaxies with optical and HI redshifts in both volumes. Magnitudes and colours from the INT observations are  $k$ -corrected and corrected for Galactic extinction. No correction for internal extinction has been applied. The HI-detected galaxies are predominantly located in the ‘blue cloud’ while a few galaxies on the ‘red sequence’ also appear gas-rich. The two brightest HI-detected galaxies are blue but at the same time as bright as the most luminous galaxies on the red sequence. These are possibly merging and star bursting galaxies but to address this issue in any detail requires a study of the UV, optical and IR imaging data.

## 5. Conclusions

We have demonstrated that observations of the HI 21cm emission line from objects at  $z \approx 0.2$  are entirely feasible with present day facilities. We have detected and measured HI emission from 160 galaxies in the redshift range 0.164–0.224 and revealed the cosmic large scale structure outlined by these 160 galaxies. The HI detected galaxies constitute a different population than the

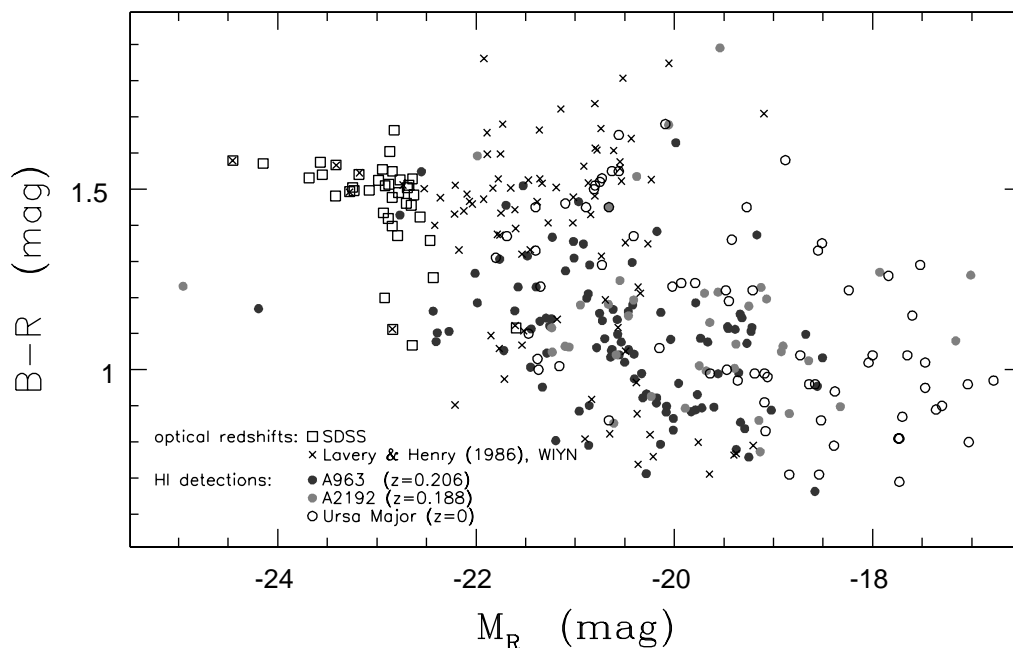


**Figure 9:** K-corrected colour-magnitude diagram of all galaxies with known redshifts (optical and HI) in both volumes. Galaxies targeted by the SDSS are mainly located at the bright tip of the 'red sequence'. HI detected galaxies are largely located within the 'blue cloud' but some HI detections have very red optical counterparts.

galaxies targeted by the SDSS for optical spectroscopy at these distances. The largest HI sources are spatially resolved by the WSRT while none of the blue galaxies that are responsible for the B-O effect in Abell 963 have been detected. There is a hint that the lower-luminosity galaxies at  $z \approx 0.2$  are more gas-rich than their counterparts at low redshift.

These WSRT observations have demonstrated that long integration times with aperture synthesis arrays can reach the expected thermal noise in the continuum subtracted channel maps. Considering the surveyed volume and the HI Mass Function in the Local Universe, the number of 160 HI detections in the WSRT survey is similar to the expected number of 200 detections, modulo cosmic variance. This provides confidence in the predicted number of HI detections in future ultra-deep surveys of HI at intermediate redshifts with new facilities like MeerKAT, APERTIF, ASKAP, EVLA, and the Square Kilometre Array.

## References

- [1] Butcher, H. & Oemler, A., Jr. 1978, *ApJ*, 219, 18
- [2] Butcher, H., Wells, D.S. & Oemler, A., Jr. 1983, *ApJS*, 52, 183
- [3] Fasano, G., Poggianti, B.M., Couch W.J., Bettoni, D., Kjaergaard, P. & Moles, M. 2000, *ApJ*, 542, 673
- [4] Verheijen, M.A.W., van Gorkom, J.H., Szomoru, A., Dwarakanath, K.S., Poggianti, B.M. & Schiminovich, D. 2007, *ApJ*, 668, L9
- [5] Verheijen, M.A.W & Sancisi, R. 2001, *A&A*, 370, 765